Higgs Decay Signal Strengths in an Extended 2HDM

Hrishabh Bharadwaj*[1], Mamta Dahiya†[2], Sukanta Dutta‡ [2,4], and Ashok Goyal§[3]

[1] *Government Mahila Degree College, Budaun, Mahatmaa Jyotiba Phule Rohilkhand University, Bareilly, 243601, Uttar Pradesh, India.*
[2] *SGTB Khalsa College, University of Delhi, Delhi, 110007, India*
[3] *Department of Physics and Astrophysics, University of Delhi, Delhi, 110007, India*
[4] *Delhi School of Analytics, Institution of Eminence, University of Delhi, Delhi, 110007, India*

Abstract

The combined CMS and ATLAS analysis of $h \to Z\gamma$ reveals a 2σ excess over the Standard Model (SM) prediction, hinting at potential new physics. In contrast, the observed agreement of $\mu_{\gamma\gamma}$ with the SM imposes stringent constraints on such extension. In this context, we investigate a Two Higgs Doublet Model (2HDM) extended by a complex scalar singlet and a vector-like lepton (VLL). This framework successfully accommodates the Higgs decay signal strengths $\mu_{W W^\star}$, $\mu_{Z\gamma}$, and $\mu_{\gamma\gamma}$ while also satisfying precision electroweak constraints, the observed experimental value of muon $g - 2$, and bounds from LEP II data. We identify a viable region of parameter space that is consistent with all low energy data and current experimental limits on the Higgs decay signal strengths.

Keywords: Higgs Decay, 2HDM , Vector Like Lepton, Muon g-2

1 Introduction

The ATLAS and CMS collaborations recently reported the first evidence for $h \to Z\gamma$ decay based on their combined analysis of LHC Run 2 datasets, with integrated luminosities of 139 fb^{-1} (ATLAS) and 138 fb^{-1} (CMS) at $\sqrt{s} = 13$ TeV. The improved combined measured signal strength is:

$$\mu_{Z\gamma}^{\text{combined}} = 2.2 \pm 0.7 \quad [1] \tag{1}$$

showing a 1.9σ excess over the Standard Model (SM) expectation. However, the signal strength for $h \to \gamma\gamma$ decay,

$$\mu_{\gamma\gamma} = 1.10 \pm 0.06 \quad [2] \tag{2}$$

aligns well with the SM prediction, imposing strong constraints on new physics explanations for the $\mu_{Z\gamma}$ excess.

Since SM corrections at the two-loop level, including QCD and electroweak effects [3, 4, 5, 6, 7, 8], are insufficient to account for this deviation, various BSM scenarios have been explored. These include multi-Higgs doublet models [9, 10, 11, 12], supersymmetry [13, 14], left-right symmetric models, ultra-light axion-like particles [15], effective field theory (EFT) approaches [16, 17], and models with off-diagonal Higgs-Z-bosons couplings [18].

Several low-energy observables show deviations from SM predictions, notably the muon anomalous magnetic moment and the CDF measurement of the W-boson mass. The latest muon $g-2$ measurement reports a 5σ discrepancy:

$$\Delta a_\mu = a_\mu^{\text{exp}} - a_\mu^{\text{SM}} = (2.49 \pm 0.08) \times 10^{-9} \quad [19, \, 20]. \tag{3}$$

While the recent CMS measurement of m_W [21] aligns with the SM, the CDF result [22, 2, 23, 24] shows a 7σ deviation, leaving the discrepancy unresolved.

To address the aforementioned discrepancies, we seek a unified framework capable of resolving these deviations. We build upon the scalar sector of the 2HDM as explored in [25, 26], where a common parameter space was identified, incorporating constraints from the muon anomalous magnetic moment, Higgs boson decays, and LEP II results. In this work, we compute the signal strength of the $h \to Z\gamma$ decay and investigate whether the parameter space required to resolve the muon $(g-2)$ anomaly remains consistent with the observed $h \to Z\gamma$ signal strength. This analysis is performed within a 2HDM framework extended by a SM-singlet complex scalar and a charged VLL. While previous studies incorporated VLL interactions, our model differs by omitting the Yukawa interactions between the VLL and right-handed SM leptons, making it distinct from the setup in [25].

This paper is organized as follows: In Section 2, we briefly describe the model. The computation of additional contributions to the Higgs decay channels $h \to \gamma\gamma$ and $h \to Z\gamma$ at the one-loop level in our model is discussed in Section 3. The numerical results for the parameter space region that simultaneously accommodates the measured signal strengths and the muon $(g-2)$ discrepancy are presented in Section 4. Finally, we summarize our findings in Section 5.

2 The Model

The extended 2HDM scalar sector includes two $SU(2)_L$ scalar doublets and a neutral singlet scalar Φ_3. The doublet Φ_1 and singlet Φ_3 acquire real vacuum expectation values (VEVs) v_{SM} and v_{s}, respectively. The scalar doublets Φ_1, Φ_2 and complex singlet ϕ_3 are defined as

$$\Phi_1 \equiv \begin{bmatrix} \phi_1^+ \\ \frac{1}{\sqrt{2}} \left(v_{\text{SM}} + \phi_1^0 + i\,\eta_1^0 \right) \end{bmatrix}, \quad \Phi_2 \equiv \begin{bmatrix} \phi_2^+ \\ \frac{1}{\sqrt{2}} \left(\phi_2^0 + i\,\eta_2^0 \right) \end{bmatrix} \quad \text{and} \quad \Phi_3 \equiv \frac{1}{\sqrt{2}} \left[v_{\text{s}} + \phi_3^0 + i\,\eta_3^0 \right],$$

$$\tag{4}$$

The scalar Lagrangian, $\mathscr{L}_{\text{scalar}}$, consists of the kinetic terms for the scalar fields along with the scalar potential.

$$\mathscr{L}_{\text{scalar}} = \sum_{i=1,2} (D_\mu \Phi_i)^\dagger \, (D^\mu \Phi_i) \, + \, (D_\mu \Phi_3)^\star \, (D_\mu \Phi_3) \, - \, V_{\text{scalar}}, \quad \text{where}$$

$$V_{\text{scalar}} = -\frac{1}{2} m_{11}^2 \left(\Phi_1^\dagger \Phi_1 \right) - \frac{1}{2} m_{22}^2 \left(\Phi_2^\dagger \Phi_2 \right) - \frac{1}{2} m_{33}^2 \, \Phi_3^* \Phi_3 + \frac{\lambda_1}{2} \left(\Phi_1^\dagger \Phi_1 \right)^2 + \frac{\lambda_2}{2} \left(\Phi_2^\dagger \Phi_2 \right)^2$$
$$+ \lambda_3 \left(\Phi_1^\dagger \Phi_1 \right) \left(\Phi_2^\dagger \Phi_2 \right) + \lambda_4 \left(\Phi_1^\dagger \Phi_2 \right) \left(\Phi_2^\dagger \Phi_1 \right) + \frac{1}{2} \left[\lambda_5 \left(\Phi_1^\dagger \Phi_2 \right)^2 + h.c. \right]$$
$$+ \frac{\lambda_8}{2} (\Phi_3^* \Phi_3)^2 + \lambda_{11} |\Phi_1|^2 \, \Phi_3^* \Phi_3 + \lambda_{13} |\Phi_2|^2 \, \Phi_3^* \Phi_3 - i\,\kappa \, \left[\left(\Phi_1^\dagger \Phi_2 + \Phi_2^\dagger \Phi_1 \right) \, (\Phi_3 - \Phi_3^\star) \right]$$

$$\tag{5}$$

A discrete Z_2 symmetry is imposed to forbid direct interactions of Φ_2 doublet with the SM fields and the Φ_1 doublet. Under this symmetry, Φ_2 and Φ_3 are assigned odd parity, whereas the SM fields and Φ_1 are even. Additionally, a global $U(1)$ symmetry is introduced under which $\Phi_3 \to e^{i\alpha}\Phi_3$, in order to reduce the number of independent parameters in the scalar potential. This symmetry is allowed to be softly broken by the κ term.

The mass matrices for neutral scalars and pseudoscalars remain decoupled due to the absence of mixing between the imaginary component of the doublet Φ_2 and the real component of either Φ_1 or Φ_3. The CP-even neutral scalar mass matrix is a 2×2 matrix that arises from the mixing of the real components of the SM-like doublet Φ_1 and the singlet Φ_3. Diagonalizing this CP-even mass matrix using an orthogonal rotation matrix parameterized by the mixing angle θ_{13} yields two mass eigenstates, h_1 and h_3. Similarly, diagonalizing the CP-odd scalar mass matrix for η_2^0 and η_3^0 using an orthogonal rotation matrix parameterized by the mixing angle θ_{23} results in the pseudoscalar mass eigenstates A^0 and P^0. For explicit expressions of the mass eigenstates and the relationships between mass parameters and scalar couplings in the Lagrangian, the reader is referred to [25, 26].

Among the remaining neutral and charged scalar mass eigenstates, η_1^0 and $\phi_1^\pm$ correspond to the massless Nambu-Goldstone bosons, while the scalars ϕ_2^0 and $\phi_2^\pm$ are now relabeled as h_2 and $H^\pm$, respectively.

The Yukawa terms for SM fields are given by:

$$-\mathscr{L}'_{\text{Yukawa}} = y_u \, \overline{Q_L} \, \widetilde{\Phi_1} \, u_R \, + \, y_d \, \overline{Q_L} \, \Phi_1 \, d_R \, + \, y_\ell \, \overline{\ell_L} \, \Phi_1 \, e_R \, + y_1 \, \overline{\ell_L} \, \Phi_2 \, e_R + \text{ h.c..} \quad (6)$$

where Q_L and ℓ_L are the quark and lepton doublets under $SU(2)_L$ gauge group. Here, the Z_2 symmetry is allowed to get softly broken in the Yukawa interactions involving Φ_2 to allow the interactions between the SM leptons with CP-odd pseudoscalars.

In addition to the scalar sector, the model includes a singlet chiral vector-like leptons, where the left-handed (right-handed) VLL is odd (even) under Z_2 symmetry. The Lagrangian for VLL is given by

$$\mathscr{L}_{\text{VLL}} = \overline{\chi} \, i \left(\slashed{\partial} - i g' \frac{Y}{2} \slashed{B} \right) \chi \, - \, m_\chi \, \overline{\chi} \, \chi - y_2 \, \overline{\chi_L} \, \chi_R \, \Phi_3 \quad (7)$$

In contrast to [25], our model excludes the y_3-induced Yukawa interactions, which previously facilitated mixing between SM fermions and the VLL. In this framework, the global $U(1)$ symmetry is allowed to be softly broken by the Yukawa coupling y_2.

The Yukawa interactions given in (6) and (7) can be re-written as:

$$-\mathscr{L}_{\text{SM Fermions}}^{\text{Yukawa}} = \sum_{s_i \equiv h_1, h_3} \frac{y_{ffs_i}}{\sqrt{2}} \left(v_{\text{SM}} \, \delta_{s_i, h_1} + s_i \right) \bar{f} \, f + \frac{y_{llh_2}}{\sqrt{2}} h_2 \bar{l}^- l^-$$

$$+ \sum_{s_i \equiv P^0, A^0} \frac{y_{lls_i}}{\sqrt{2}} s_i \bar{l}^- \gamma_5 \, l^- + \left[y_{l\nu H^-} \, \bar{\nu}_l \, P_R \, l^- \, H^+ + \text{h.c.} \right], \quad (8)$$

$$-\mathscr{L}_{\text{VL Leptons}}^{\text{Yukawa}} = \sum_{s_i \equiv h_1, h_3, A^0, P^0} \frac{1}{\sqrt{2}} \left(v_s \, \delta_{s_i, h_3} + s_i \right) \bar{\chi} \left(y_{\chi\chi s_i} P_R + y^\star_{\chi\chi s_i} P_L \right) \chi, \quad (9)$$

where f and l^- denote SM fermions and SM charged leptons, respectively, and y's represent the couplings of the fermionic fields (f, l, ν, χ) with the charged or neutral scalar/ pseudoscalar mass eigenstates. These Yukawa couplings depend on the vacuum expectation values (VEVs), the parameters y_i (for $i = 1, 2$), and the mixing angles θ_{13} and θ_{23}. The explicit expressions for these couplings can be found in Table 1 of [25].

There are 12 parameters in the scalar potential (5), namely, $v_s, m_{11}, m_{22}, m_{33}, \lambda_{i=1,3,4,5,8,11,13}$ and κ. Among these, the parameter λ_2 does not contribute to the mass spectrum and is therefore not constrained by our analysis. Additionally, v_s and m_{22} are not directly constrained. The eight dimensionless couplings in the scalar potential and Yukawa sector are assumed to be real to preserve CP invariance. Thus, along with the Yukawa couplings y_i, we consider the effects of the following 13 physical parameters in our study:

$$\begin{aligned} \text{Masses} \quad &: \quad m_{h_1}, m_{h_2}, m_{h_3}, m_{H^\pm}, \, m_{A^0}, m_{P^0}, \, m_\chi \\ \text{Mixing Angles} \quad &: \quad \theta_{13}, \theta_{23} \\ \text{Couplings} \quad &: \quad y_1, y_2, \lambda_{h_1 H^+ H^-}, \lambda_{h_3 H^+ H^-} \end{aligned} \quad (10)$$

where $\lambda_{h_1 H^+ H^-}$ and $\lambda_{h_3 H^+ H^-}$ are the dimensionless scalar triple couplings of the charged Higgs bosons with neutral scalars, given by

$$\lambda_{h_1 H^+ H^-} = \lambda_3 \cos\theta_{13} + \frac{v_s}{v_{\text{SM}}} \lambda_{13} \sin\theta_{13} \quad \text{and} \quad \lambda_{h_3 H^+ H^-} = \frac{v_s}{v_{\text{SM}}} \lambda_{13} \cos\theta_{13} - \lambda_3 \sin\theta_{13} \quad (11)$$

The co-positivity conditions impose mutually exclusive allowed regions for λ_4 and λ_5 [25, 26], leading to :

$$\Theta(|\lambda_5| - \lambda_4) = \begin{cases} \Theta\left[m_{H^\pm}^2 - (m_{A^0}^2 + m_{P^0}^2)\right] & \text{for } m_{h_2}^2 > m_{A^0}^2 + m_{P^0}^2 \\ \Theta\left[m_{h_2}^2 - m_{H^\pm}^2\right] & \text{for } m_{h_2}^2 < m_{A^0}^2 + m_{P^0}^2 \end{cases} \quad (12)$$

In this article, we explore the phenomenologically interesting region where $m_{H^\pm}^2$ and $m_{h_2}^2$ are $> m_{A^0}^2 + m_{P^0}^2$. For further analysis, all Yukawa couplings are restricted to the range $|y_i| \le \sqrt{4\pi}$ as required by tree-level perturbative unitarity.

3 Higgs Decay Signal Strengths

Any multi-Higgs model must accommodate an SM-like Higgs boson with the mass and signal strengths measured at the LHC. The LHC data favor a scalar eigenstate h^{SM} with a mass of approximately 125 GeV [2]. This motivates us to identify the lightest CP-even neutral scalar, h_1, with the observed Higgs boson and set $m_{h_1} = 125$ GeV. Furthermore, the couplings of h_1 to fermions and gauge bosons are the corresponding SM Higgs couplings, suppressed by a factor of $\cos\theta_{13}$ due to $\Phi_1 - \Phi_3$ mixing.

Signal strength is a key observable used to quantify the deviation of the observed signal from the SM expectation in specific decay channels. To constrain the parameter space of the model through Higgs decays, we require that h_1 decays account for the measured total Higgs decay width. For this purpose, we define the signal strength μ_{XY} relative to h^{SM} production via the dominant gluon fusion process in $p-p$ collisions, followed by its decay into X, Y pairs, under the narrow width approximation:

$$\mu_{XY} = \frac{\sigma(pp \to h_1 \to XY)}{\sigma(pp \to h \to XY)^{\text{SM}}} = \frac{\Gamma(h_1 \to gg)}{\Gamma(h^{SM} \to gg)} \times \frac{\text{BR}(h_1 \to XY)}{\text{BR}(h^{\text{SM}} \to XY)} = \cos^2\theta_{13} \times \frac{\text{BR}(h_1 \to XY)}{\text{BR}(h^{\text{SM}} \to XY)}.$$
$$(13)$$

3.1 $h_1 \to WW^\star$

The partial decay width of $h_1 \to WW^\star$ channel in our model is related to the corresponding SM value as

$$\Gamma(h_1 \to WW^\star) = \cos^2\theta_{13}\, \Gamma(h^{\text{SM}} \to WW^\star). \quad (14)$$

Using

$$\begin{aligned} \Gamma(h^{\text{SM}} \to \text{all}) &= (4.07 + 4\% - 3.9\%)\, \text{GeV} \simeq 4.07 \pm 0.163\, \text{GeV}, \\ \text{and} \quad \Gamma(h^{\text{SM}} \to \text{all})_{\text{LHC}} &= 3.7^{+1.9}_{-1.4}\, \text{GeV} \end{aligned} \quad (15)$$

from reference [2], the corresponding signal strength is given by

$$\mu_{WW^\star} = \cos^4\theta_{13}\, \frac{\Gamma(h^{\text{SM}} \to \text{all})}{\Gamma(h^{\text{SM}} \to \text{all})_{\text{LHC}}} \simeq (1.1 \pm 0.57)\cos^4\theta_{13} \quad (16)$$

Thus, the signal strength $\mu_{WW^\star}$ depends only on the parameter θ_{13}, which can be strongly constrained by the observed value, from the LHC, $\mu_{WW^\star} = 1.00 \pm 0.08$ [2]. Using the central value of $\mu_{WW^\star}$ from (16), we get $0.92 \le 1.1\cos^4\theta_{13} \le 1.08$, resulting in the allowed range of θ_{13} to be

$$5.5° \le \theta_{13} \le 17°. \quad (17)$$

3.2 $h_1 \to \gamma\gamma$ and $h_1 \to Z\gamma$

The partial decay widths for $h_1 \to \gamma\gamma$ and $h_1 \to Z\gamma$ are generated at the one-loop level through the contributions of charged scalar $H^\pm$ and vector-like lepton χ, and are parameterized in our model as

$$\Gamma(h_1 \to \gamma\,\gamma) = \cos^2\theta_{13}\,|1 + \zeta_{\gamma\gamma}|^2\,\Gamma\left(h^{\rm SM} \to \gamma\,\gamma\right), \tag{18}$$

$$\Gamma(h_1 \to Z\,\gamma) = \cos^2\theta_{13}\,|1 + \zeta_{Z\gamma}|^2\,\Gamma\left(h^{\rm SM} \to Z\,\gamma\right). \tag{19}$$

where the SM Higgs partial decay widths in $\gamma\,\gamma$ and $Z\,\gamma$ channels are given as:

$$\Gamma(h^{\rm SM} \to \gamma\gamma) = \frac{G_F\alpha^2\,m_h^3}{128\sqrt{2}\pi^3}\left|\frac{4}{3}\mathscr{M}_{1/2}^{\gamma\gamma}\left(\frac{4m_t^2}{m_{h^{\rm SM}}^2}\right) + \mathscr{M}_1^{\gamma\gamma}\left(\frac{4m_{\rm W}^2}{m_{h^{\rm SM}}^2}\right)\right|^2 \tag{20}$$

$$\Gamma(h^{\rm SM} \to Z\gamma) = \frac{G_F^2\,\alpha\,m_W^2\,m_h^3}{64\,\pi^4}\left(1 - \frac{m_Z^2}{m_{h^{\rm SM}}^2}\right)^3$$
$$\times\left|2\frac{\left(1 - \frac{8}{3}s_W^2\right)}{c_W}\mathscr{M}_{1/2}^{Z\gamma}\left(\frac{4m_t^2}{m_{h^{\rm SM}}^2}, \frac{4m_t^2}{m_Z^2}\right) + \mathscr{M}_1^{Z\gamma}\left(\frac{4m_W^2}{m_{h^{\rm SM}}^2}, \frac{4m_W^2}{m_Z^2}\right)\right|^2. \tag{21}$$

The dimensionless parameters $\zeta_{\gamma\gamma}$ and $\zeta_{Z\gamma}$ are defined as:

$$\zeta_{\gamma\gamma} = \frac{v_{\rm SM}}{\cos\theta_{13}}\left[\frac{\frac{g_{h_1 H^+ H^-}}{2\,m_{H^\pm}^2}\mathscr{M}_0^{\gamma\gamma}\left(\frac{4m_{H^\pm}^2}{m_{h_1}^2}\right) + \frac{y_2}{\sqrt{2}m_\chi}\sin\theta_{13}\mathscr{M}_{1/2}^{\gamma\gamma}\left(\frac{4\,m_\chi^2}{m_{h_1}^2}\right)}{\mathscr{M}_1^{\gamma\gamma}\left(\frac{4\,m_W^2}{m_{h_1}^2}\right) + \frac{4}{3}\mathscr{M}_{1/2}^{\gamma\gamma}\left(\frac{4\,m_t^2}{m_{h_1}^2}\right)}\right] \tag{22}$$

$$\zeta_{Z\gamma} = \frac{v_{\rm SM}}{\cos\theta_{13}}\left[\frac{-\frac{g_{h_1 H^+ H^-}}{2m_{H^\pm}^2}\frac{1-2s_W^2}{c_{\theta_W}}\mathscr{M}_0^{Z\gamma}\left(\frac{4m_{H^\pm}^2}{m_{h_1}^2}, \frac{4m_{H^\pm}^2}{m_Z^2}\right) - \frac{y_2}{\sqrt{2}m_\chi}\sin\theta_{13}\frac{4\,s_W^2}{c_W}\mathscr{M}_{1/2}^{Z\gamma}\left(\frac{4m_\chi^2}{m_{h_1}^2}, \frac{4m_\chi^2}{m_Z^2}\right)}{2\frac{(1-\frac{8}{3}s_W^2)}{c_W}\mathscr{M}_{1/2}^{Z\gamma}\left(\frac{4m_t^2}{m_{h_1}^2}, \frac{4m_t^2}{m_Z^2}\right) + \mathscr{M}_1^{Z\gamma}\left(\frac{4m_W^2}{m_{h_1}^2}, \frac{4m_W^2}{m_Z^2}\right)}\right]. \tag{23}$$

where $g_{h_1 H^+ H^-} = v_{\rm SM}\lambda_{h_1 H^+ H^-}$. For the loop amplitudes $\mathscr{M}_{0,1/2,1}^{\gamma\gamma}$ and $\mathscr{M}_{0,1/2,1}^{Z\gamma}$, the reader is referred to the reference [25]. Using the relations (13), (14), and (19), the ratios of signal strengths may be written as

$$\frac{\mu_{\gamma\gamma(Z\gamma)}}{\mu_{WW^\star}} = \frac{\Gamma\left(h_1 \to \gamma\,\gamma(Z\gamma)\right)}{\Gamma\left(h^{\rm SM} \to \gamma\,\gamma(Z\gamma)\right)} \times \frac{\Gamma(h^{\rm SM} \to WW^\star)}{\Gamma(h_1 \to W\,W^\star)} = \left|1 + \zeta_{\gamma\gamma(Z\gamma)}\right|^2 \tag{24}$$

4 Numerical Analysis

4.1 Higgs Decay Signal Strengths

The signal strengths $\mu_{\gamma\gamma}$ and $\mu_{Z\gamma}$ depend on five key model parameters: $|\theta_{13}|$, $\lambda_{h_1 H^+ H^-}$, y_2, $m_{H^\pm}$, and m_χ. Among these, θ_{13} is already constrained by $\mu_{WW^\star}$ as specified in equation (17). The negative values of θ_{13} are taken into account by changing the sign of the coupling y_2 in the computation of both $\mu_{\gamma\gamma}$ and $\mu_{Z\gamma}$. Accordingly, we fix $|\theta_{13}|$ to three representative values: $5.5°$, $10°$, and $15°$, and compute the one loop contributions to $\mu_{\gamma\gamma}$ and $\mu_{Z\gamma}$ by scanning the remaining parameters over the ranges: $\lambda_{h_1 H^+ H^-} \in [-10 : 10]$, $y_2 \in [-3.5 : 3.5]$, $m_\chi \in [200 : 1000]$ GeV, and $m_{H^\pm} \in [\sqrt{m_{A^0}^2 + m_{P^0}^2} : 1000]$ GeV. Figure 1a (1b) presents the density distribution of the coupling y_2 ($\lambda_{h_1 H^+ H^-}$) in the $m_{H^\pm} - m_\chi$ plane, consistent with the observed $\mu_{\gamma\gamma}$ and $\mu_{Z\gamma}$ signal strengths within the 2σ experimental range. The color bar indicates the range of y_2 ($\lambda_{h_1 H^+ H^-}$), where positive and negative values are distributed across different mass regions. The structured density regions indicate strong correlations between these couplings and the Higgs decay constraints. The figure 2 gives the parameter region consistent with all three
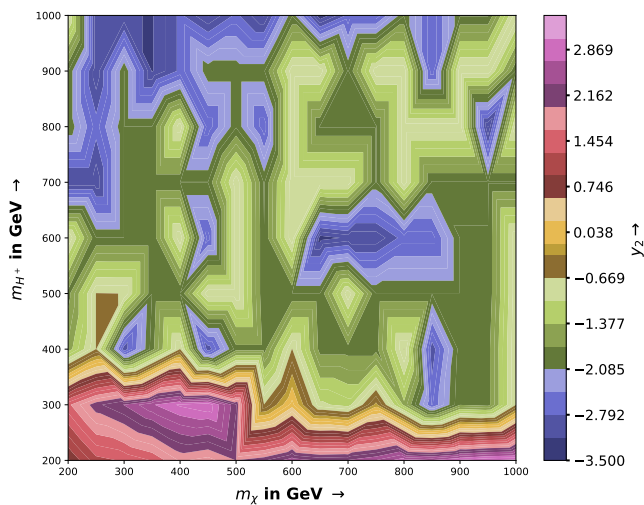
(a) y_2 contours and density map in the $m_{H^\pm} - m_\chi$ plane
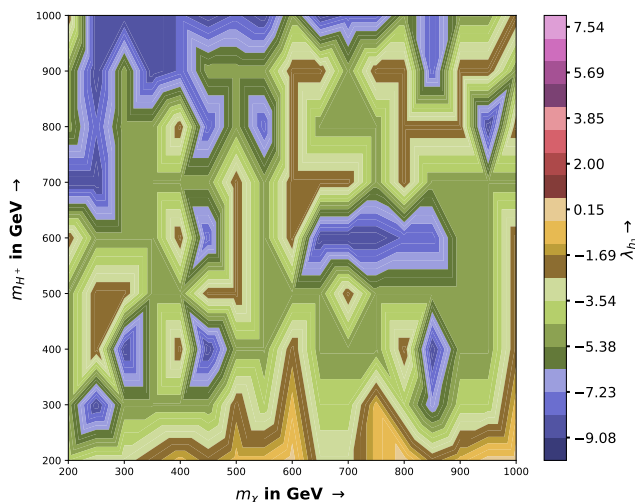
(b) $\lambda_{h_1 H^+ H^-}$ contours and density map in the $m_{H^\pm} - m_\chi$ plane

Figure 1: *Density maps of couplings y_2 and $\lambda_{h_1 H^+ H^-}$ in the $m_{H^\pm} - m_\chi$ plane. The contours represent parameter regions consistent with the observed Higgs decay signal strengths $\mu_{Z\gamma}$ and $\mu_{\gamma\gamma}$ at the 2σ level.*

signal strengths, namely, $\mu_{Z\gamma}$, $\mu_{\gamma\gamma}$ and $\mu_{WW^\star}$, at the 2σ level. We find that $\mu_{Z\gamma}$ is strongly dependent on $\mu_{WW^\star}$, while $\mu_{\gamma\gamma}$ varies slowly with $\mu_{WW^\star}$, especially for lower values of $\mu_{Z\gamma}$. Furthermore, a natural cut-off on $\mu_{Z\gamma}$ appears for a given $\mu_{\gamma\gamma}$ and $\mu_{WW^\star}$, as depicted by the right edge in figure 2.

4.2 Model constraints

We now proceed to constrain our model parameter space using (i) existing LEP II data, (ii) precision observables ΔS and ΔT, and (iii) the muon anomalous magnetic moment. The DEL-PHI and L3 combined analysis at LEP II ($\sqrt{s} = 200$ GeV) estimates the muon pair production
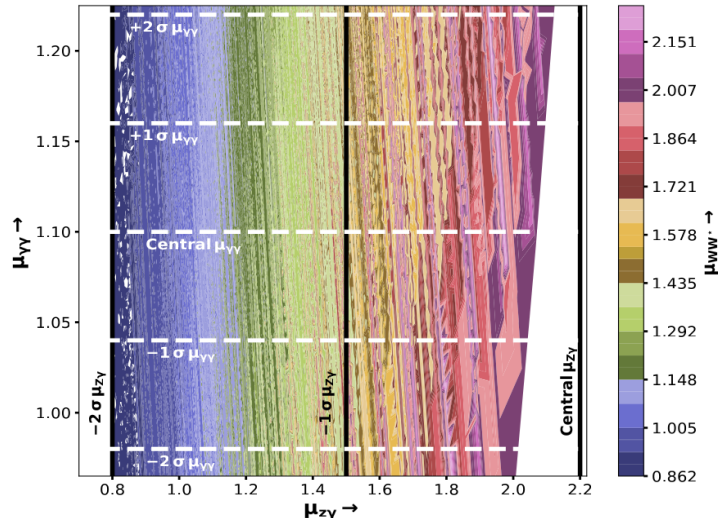
Figure 2: *Density plot of Higgs decay signal strength μ_{WW} in $\mu_{Z\gamma}$-$\mu_{\gamma\gamma}$ plane. The white dashed lines denote the $\pm 1\sigma$ and $\pm 2\sigma$ confidence levels for $\mu_{\gamma\gamma}$, with the central value highlighted. The pair of thick black lines denote the -2σ and -1σ values for $\mu_{Z\gamma}$.*

cross-section as [27]

$$\sigma(e^+ \, e^- \to \mu^+ \, \mu^-) = 3.072 \pm 0.108 \pm 0.018 \, \text{pb}. \tag{25}$$

The excess contribution to this cross-section, beyond the SM prediction, arises from the $|y_1|$-induced Yukawa interactions between SM fermions and neutral scalars/ pseudoscalars [25, 26].

While LEP II constraints do not directly impact $\mu_{\gamma\gamma}$ and $\mu_{Z\gamma}$, they significantly influence the parameters used to compute deviations ΔS and ΔT, arising from radiative corrections due to extra scalars, pseudoscalars, and VLL contributions in SM gauge boson self-energies. The corrections are evaluated over a parameter space constrained by LEP II data and are required to lie within the 1σ experimental uncertainties:

$$\Delta S = -0.01 \pm 0.07, \quad \Delta T = 0.04 \pm 0.06 \quad [2]. \tag{26}$$

thereby imposing additional constraints on the model parameter space.

Next, we explore viable regions within the filtered model parameter sets to account for the observed anomalous magnetic dipole moment of the muon, as given by (3). To this end, we compute the one-loop and dominant two-loop Barr-Zee contributions to the muon's anomalous magnetic moment within our model and subtract the SM contributions.

The resulting deviation, Δa_μ, arises from the exchange of additional VLLs as well as charged and neutral scalars and pseudoscalars (for details, see reference [25]). Requiring this excess contribution to remain within the 1σ uncertainty of the observed muon anomalous magnetic moment further shrinks the model's parameter space.

Finally, using the screened parameter sets, we compute $\mu_{\gamma\gamma}$ and $\mu_{Z\gamma}$ demonstrating the simultaneous explanation of both signal strengths while satisfying all the low energy constraints.

Due to paucity of space, we illustrate the existence of a viable region by selecting four sets of (m_{A^0}, m_{P^0}): (150, 300) GeV, (300, 150) GeV, (150, 150) GeV, and (150, 450) GeV. For each of these choices, we scan the remaining parameters to compute the $\mu_{\gamma\gamma}$ and $\mu_{Z\gamma}$, ensuring consistency with key low-energy constraints as discussed in the previous section. The parameters are varied within the following ranges:
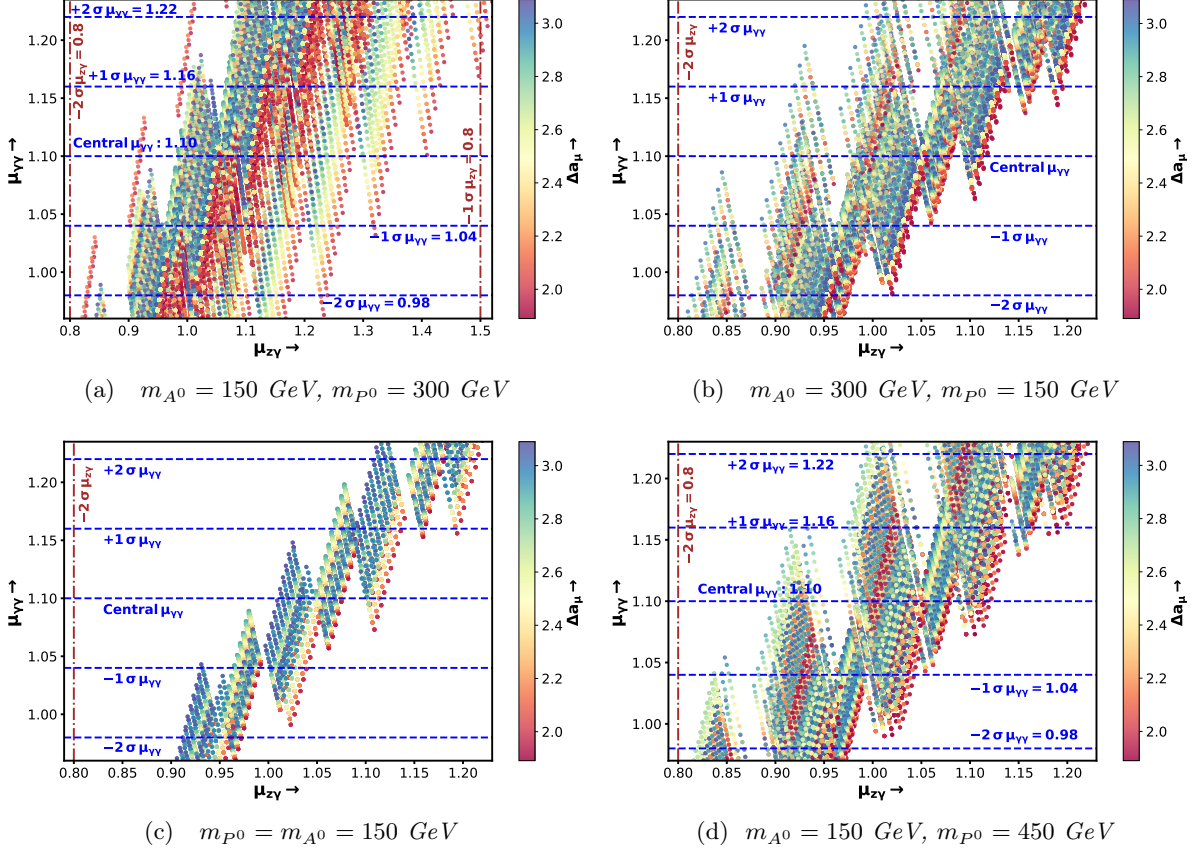
7

Figure 3: *Scatter Plots depicting the combined solution consistent with signal strengths $\mu_{Z\gamma}, \mu_{\gamma\gamma}$ at 2σ level and muon $g-2$ at 1σ with the parameter space constrained by (i) μ_{WW^*}, (ii) $\sigma(e^+ e^- \to \mu^+ \mu^-)$ from LEP, and (iii) oblique parameters $\Delta S, \Delta T$ at 1σ. The plots are shown for specific values of m_{A^0}, m_{P^0} as mentioned. All other parameters are scanned in the range as given in section 4.2.*

- Mixing Angles: $|\theta_{13}| = 5.5°, 10°$, and $15°$, alongwith $15° \leq |\theta_{23}| \leq 90°$.
  Note that negative values of θ_{13} and θ_{23} are effectively incorporated by appropriately adjusting the signs of the couplings $\lambda_{h_1 H^+ H^-}$ and y_2 in the computation of both the Higgs signal strengths and the anomalous magnetic moment of muon.

- Couplings: $-10 < \lambda_{h_1 H^+ H^-} < 10$,   and $-10 < \lambda_{h_3 H^+ H^-} < 10$.

- Masses:
  (i) $\sqrt{m_{A^0}^2 + m_{P^0}^2} < m_{h_2}, m_{H^\pm} < 1000$ GeV,   (ii) $250 < m_{h_3} < 1000$ GeV,   and   (iii) $m_\chi \in [200, 1000]$ GeV.

The results of this analysis are encapsulated in Figure 3, where the four scatter plots display the viable regions in $\mu_{Z\gamma}$ - $\mu_{\gamma\gamma}$ plane. These regions satisfy the 2σ bounds from the combined CMS and ATLAS analyses while also incorporating constraints from the Higgs signal strength μ_{WW^*}, LEP bounds on $\sigma(e^+e^- \to \mu^+\mu^-)$, and the electroweak oblique parameters ΔS, ΔT. Each panel corresponds to a distinct benchmark choice of (m_{A^0}, m_{P^0}), while the color bar encodes the contribution to the muon anomalous magnetic moment Δa_μ, constrained within its 1σ experimental range. We observe that

- The viable parameter space forms structured, diagonal bands, indicative of a strong correlation between $\mu_{Z\gamma}$ and $\mu_{\gamma\gamma}$, which stem from shared underlying parameter dependencies.

- The high-density regions in the scatter plots, where numerous viable points cluster, indicate parameter configurations that most consistently satisfy all experimental constraints, highlighting the most robust areas of the model's viable parameter space.

- The solutions tend to cluster near the central value of $\mu_{\gamma\gamma}$, while showing a preference for $\mu_{Z\gamma} \lesssim 1.5$, which lies below the current central experimental value of 2.2. Should future measurements shift the experimental $\mu_{Z\gamma}$ closer to the SM prediction, the model's viability would be further strengthened.

5 Summary

We have investigated the parameter space of a constrained 2HDM extended by a complex scalar singlet and a VLL, incorporating constraints from LEP II data, electroweak precision observables (ΔS, ΔT), and the muon anomalous magnetic moment Δa_μ.

A detailed numerical scan over the model parameters, including mixing angles, scalar quartic couplings, and mass eigenvalues within experimentally allowed intervals, reveals sizable regions of the model parameter space that are consistent with the observed Higgs boson decay signal strengths $\mu_{\gamma\gamma}$ and $\mu_{Z\gamma}$ within their two sigma experimental ranges. As shown in Figure 3, these viable regions also satisfy the constraints from the muon $(g-2)_\mu$ anomaly, along with electroweak precision bounds and LEP II exclusion limits. These results demonstrate that the model offers a phenomenologically viable framework capable of addressing current experimental anomalies while maintaining consistency with all relevant precision observables.

Acknowledgements

References

[1] G. Aad *et al.* [ATLAS and CMS], "Evidence for the Higgs Boson Decay to a Z Boson and a Photon at the LHC," Phys. Rev. Lett. **132**, no.2, 021803 (2024) doi:10.1103/PhysRevLett.132.021803 [arXiv:2309.03501 [hep-ex]].

[2] Navas, S. and others (Particle Data Group), "Review of particle physics," Phys. Rev. D **110**, no.3, 030001 (2024), doi:10.1103/PhysRevD.110.030001.

[3] M. Spira, A. Djouadi and P. M. Zerwas, "QCD corrections to the H Z gamma coupling," Phys. Lett. B **276**, 350–353 (1992) doi:10.1016/0370-2693(92)90331-W.

[4] H. Belusca-Maito, "Higgs Couplings in an Effective Theory Framework," [arXiv:1507.05657 [hep-ph]].

[5] T. Gehrmann, S. Guns and D. Kara, "The rare decay $H \to Z\gamma$ in perturbative QCD," JHEP **09**, 038 (2015) doi:10.1007/JHEP09(2015)038 [arXiv:1505.00561 [hep-ph]].

[6] F. Buccioni, F. Devoto, A. Djouadi, J. Ellis, J. Quevillon and L. Tancredi, "Interference effects in $gg \to H \to Z\gamma$ beyond leading order," Phys. Lett. B **851**, 138596 (2024) doi:10.1016/j.physletb.2024.138596 [arXiv:2312.12384 [hep-ph]].

[7] Z. Q. Chen, L. B. Chen, C. F. Qiao and R. Zhu, "Two-loop electroweak corrections to the Higgs boson rare decay process $H \to Z\gamma$," Phys. Rev. D **110**, no.5, L051301 (2024) doi:10.1103/PhysRevD.110.L051301 [arXiv:2404.11441 [hep-ph]].

[8] W. L. Sang, F. Feng and Y. Jia, "Next-to-leading-order electroweak correction to $H \to Z0\gamma$," Phys. Rev. D **110**, no.5, L051302 (2024) doi:10.1103/PhysRevD.110.L051302 [arXiv:2405.03464 [hep-ph]].

[9] S. Panghal and B. Mukhopadhyaya, "Loop-induced Higgs decays in two Higgs doublet scenarios: some observations," [arXiv:2310.04136 [hep-ph]].

[10] A. Arhrib, K. H. Phan, V. Q. Tran and T. C. Yuan, "When Standard Model Higgs Meets Its Lighter 95 GeV Higgs," [arXiv:2405.03127 [hep-ph]].

[11] A. Arhrib, R. Benbrik, L. Rahili, S. Semlali and B. Taki, "Echoes of Veltman criteria on the next-two-Higgs-doublet model," Eur. Phys. J. C **84**, no.8, 799 (2024) doi:10.1140/epjc/s10052-024-13186-7 [arXiv:2406.13001 [hep-ph]].

[12] F. Z. Chen, Q. Wen and F. Xu, "Confronting $h \to Z\gamma$ Excess with the Two Higgs Doublet Model," [arXiv:2412.18540 [hep-ph]].

[13] H. C. Hu, Z. Y. Zhang, N. Y. Zhu and H. X. Chen, "Higgs boson decays $h \to MZ$ in the TNMSSM*," Chin. Phys. C **48**, no.9, 093101 (2024) doi:10.1088/1674-1137/ad5427 [arXiv:2406.00946 [hep-ph]].

[14] S. Israr and M. Rehman, "Higgs Decay to $Z\gamma$ in the Minimal Supersymmetric Standard Model and Its Nonholomorphic Extension," [arXiv:2407.01210 [hep-ph]].

[15] Cheung, Kingman and Ouseph, C. J., "Interpretation of excess in $H \to Z\gamma$ using a light axionlike particle", arXiv:2402.05678 [hep-ph], Phys. Rev. D **110**, 055016 (2024), doi:10.1103/PhysRevD.110.055016.

[16] He, Xiao-Gang and Huang, Zhong-Lv and Li, Ming-Wei and Liu, Chia-Wei, "The SM expected branching ratio for $h \to \gamma\gamma$ and an excess for $h \to \gamma$", arXiv:2402.08190 [hep-ph], JHEP **10**, 135 (2024), doi:10.1007/JHEP10(2024)135.

[17] Mantzaropoulos, Kostas, "Disentangling SMEFT and UV contributions in $h \to Z\gamma$ and $h \to \gamma\gamma$ decays", arXiv:2407.09145 [hep-ph], Phys. Rev. D **110**, 055041 (2024), doi:10.1103/PhysRevD.110.055041.

[18] Boto, Rafael and Das, Dipankar and Romao, Jorge C. and Saha, Ipsita and Silva, Joao P., "New physics interpretations for nonstandard values of $h \to Z\gamma$", arXiv:2312.13050 [hep-ph], Phys. Rev. D **109**, 095002 (2024), doi:10.1103/PhysRevD.109.095002.

[19] Aguillard, D. P. et al. [Muon g-2 Collaboration], "Measurement of the Positive Muon Anomalous Magnetic Moment to 0.20 ppm", arXiv:2308.06230 [hep-ex], Phys. Rev. Lett. **131**, 161802 (2023), doi:10.1103/PhysRevLett.131.161802.

[20] T. Aoyama et al., "The anomalous magnetic moment of the muon in the Standard Model", Phys. Rep. **887**, 1-166 (2020), doi:10.1016/j.physrep.2020.07.006, arXiv:2006.04822 [hep-ph], https://www.sciencedirect.com/science/article/pii/S0370157320302556.

[21] CMS Collaboration, "Measurement of the W boson mass in proton-proton collisions at $\sqrt{s}$ = 13 TeV", CMS-PAS-SMP-23-002 (2024), https://cds.cern.ch/record/2910372.

[22] Aaltonen, T. et al. [CDF Collaboration], "High-precision measurement of the W boson mass with the CDF II detector", Science **376**, 170–176 (2022), doi:10.1126/science.abk1781.

[23] Amoroso, Simone and others (LHC-TeV MW Working Group), "Compatibility and combination of world W-boson mass measurements," Eur. Phys. J. C **84**, no.5, 451 (2024), doi:10.1140/epjc/s10052-024-12532-z, arXiv:2308.09417 [hep-ex].

[24] de Blas, J., Pierini, M., Reina, L., and Silvestrini, L., "Impact of the Recent Measurements of the Top-Quark and W-Boson Masses on Electroweak Precision Fits," Phys. Rev. Lett. **129**, no.27, 271801 (2022), doi:10.1103/PhysRevLett.129.271801, arXiv:2204.04204 [hep-ph].

[25] Bharadwaj, Hrishabh, Dutta, Sukanta, and Goyal, Ashok, "Leptonic g-2 anomaly in an extended Higgs sector with vector-like leptons," JHEP **11**, 056 (2021), doi:10.1007/JHEP11(2021)056, arXiv:2109.02586 [hep-ph].

[26] Bharadwaj, Hrishabh, Dahiya, Mamta, Dutta, Sukanta, and Goyal, Ashok, "W mass and muon g-2 in an inert 2HDM extended by a singlet complex scalar," Phys. Rev. D **110**, no.11, 115040 (2024), doi:10.1103/PhysRevD.110.115040, arXiv:2407.00181 [hep-ph].

[27] Schael, S. and others (ALEPH, DELPHI, L3, OPAL, LEP Electroweak), "Electroweak Measurements in Electron-Positron Collisions at W-Boson-Pair Energies at LEP," Phys. Rept. **532**, 119–244 (2013), doi:10.1016/j.physrep.2013.07.004, arXiv:1302.3415 [hep-ex].